RSC Advances

PAPER

View Article Online
View Journal | View Issue

Check for updates

Cite this: *RSC Adv.*, 2020, **10**, 44785

Spin–orbit coupling effect on electronic, optical, and thermoelectric properties of Janus Ga_2SSe

Hong T. T. Nguyen,[ab] Vo T. T. Vi,[cd] Tuan V. Vu,[ab] Nguyen V. Hieu,*[e] Dung V. Lu,*[e] D. P. Rai[f] and Nguyen T. T. Binh[gh]

In this paper, we investigate the electronic, optical, and thermoelectric properties of Ga_2SSe monolayer by using density functional theory. *Via* analysis of the phonon spectrum and *ab initio* molecular dynamics simulations, Ga_2SSe is confirmed to be stable at room temperature. Our calculations demonstrate that Ga_2SSe exhibits indirect semiconductor characteristics and the spin–orbit coupling (SOC) effect has slightly reduced its band gap. Besides, the band gap of Ga_2SSe depends tightly on the biaxial strain. When the SOC effect is included, small spin–orbit splitting energy of 90 meV has been found in the valence band. However, the spin–orbit splitting energy dramatically changes in the presence of biaxial strain. Ga_2SSe exhibits high optical absorption intensity in the near-ultraviolet region, up to 8.444×10^4 cm^{-1}, which is needed for applications in optoelectronic devices. By using the Boltzmann transport equations, the electronic transport coefficients of Ga_2SSe are comprehensively investigated. Our calculations reveal that Ga_2SSe exhibits a very low lattice thermal conductivity and high figure of merit *ZT* and we can enhance its *ZT* by temperature. Our findings provide further insight into the physical properties of Ga_2SSe as well as point to prospects for its application in next-generation high-performance devices.

Received 28th September 2020
Accepted 25th November 2020

DOI: 10.1039/d0ra08279a

rsc.li/rsc-advances

Open Access Article. Published on 17 December 2020. Downloaded on 7/16/2025 6:28:26 AM.
This article is licensed under a Creative Commons Attribution-NonCommercial 3.0 Unported Licence.

1 Introduction

The physical properties of two-dimensional (2D) materials are very sensitive to the perfection of the atomic structure.[1–3] The breaking of symmetrical structures in 2D materials can offer new physical properties with many potentials for applications in technology. Motivated by this view, the Janus asymmetric structure MoSSe has been experimentally reported recently.[4,5] Compared with MoS_2 or $MoSe_2$, there is a lack of mirror symmetry in the Janus structure MoSSe and out-of-plane structural asymmetry in MoSSe has been identified by spectroscopy.[4] The successful synthesis of Janus MoSSe opened a new chapter in the research for the 2D family and many different types of Janus structures were theoretically studied recently.[6–9]

Janus structures show a high prospect for use as thermoelectric materials due to their owning a high thermoelectric figure of merit.[10] With suitable band edge alignment, Janus structures are expected to be used in photocatalytic water splitting.[11] By using density functional theory (DFT) calculations, Yao and co-workers have revealed that mirror symmetry breaking in Janus MoSSe structure induces a very large Rashba spin splitting.[12] Also, one can modulate the electronic properties of Janus monolayers by an applied strain[13] or external electric field.[14] Recent DFT calculations demonstrated that MoSeTe possesses high absorption intensity and becoming a great candidate for applications in optoelectronic devices.[15] Recently, van der Waals heterostructures based Janus monolayers have been studied with a lot of attention.[7,16,17] In graphene/Ga_2SSe heterostructures, a small band gap has been found in graphene due to weak interactions between graphene and Ga_2SSe.[17] It implies that forming heterostructures with the Janus structure is one of the ways to overcome the gapless disadvantage of graphene.

Excited by the successes in studies of Janus dichalcogenides, Janus monochalcogenides structures, especially Janus structures based on group III–VI compounds, have gained attention recently.[11,18] Wan and co-workers indicated that the Janus In_2SeTe exhibits higher carrier mobility that of InSe.[19] Also, strain engineering is one of the good ways to modulate the thermal conductivity of InSe-based Janus.[19] Using DFT calculations, Gou

[a]*Division of Computational Physics, Institute for Computational Science, Ton Duc Thang University, Ho Chi Minh City, Vietnam. E-mail: nguyenthithamhong@tdtu.edu.vn; vuvantuan@tdtu.edu.vn*

[b]*Faculty of Electrical & Electronics Engineering, Ton Duc Thang University, Ho Chi Minh City, Vietnam*

[c]*Department of Physics, University of Education, Hue University, Hue, Vietnam*

[d]*Department of Fundamental Sciences, University of Medicine and Pharmacy, Hue University, Hue, Vietnam*

[e]*Faculty of Physics, The University of Danang – University of Science and Education, Da Nang, Vietnam. E-mail: nvhieu@ued.udn.vn; dvlu@ued.udn.vn*

[f]*Department of Physics, Physical Sciences Research Center, Pachhunga University College, Aizawl 796001, India*

[g]*Institute of Research and Development, Duy Tan University, Da Nang 550000, Vietnam. E-mail: nguyentthanhbinh8@duytan.edu.vn*

[h]*Faculty of Natural Sciences, Duy Tan University, Da Nang 550000, Vietnam*

Open Access Article. Published on 17 December 2020. Downloaded on 7/16/2025 6:28:26 AM.
This article is licensed under a Creative Commons Attribution-NonCommercial 3.0 Unported Licence.

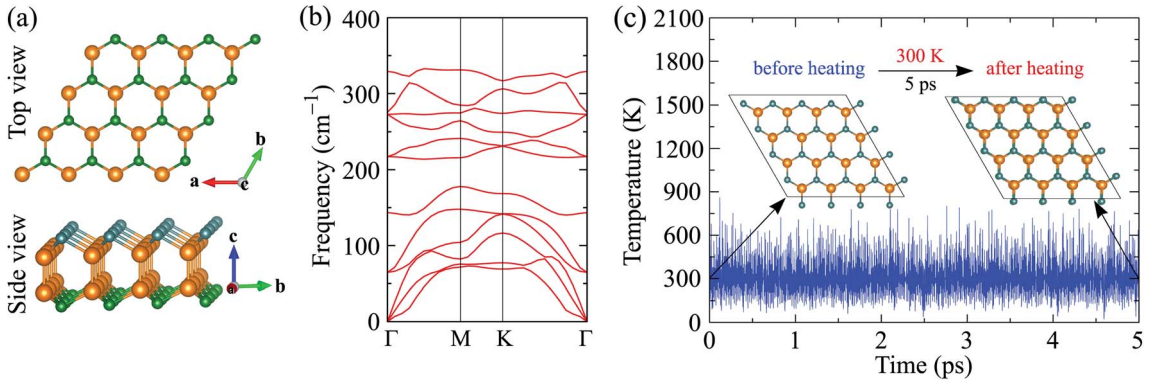

Fig. 1 (a) Geometric structure, (b) phonon dispersion, and (c) time-dependent AIMD simulations of temperature fluctuation at room temperature of Ga_2SSe monolayer. Insets in (c) are the atomic structures of Ga_2SSe before and after heat-treatment of 5 ps.

et al. have shown that the Janus group III monochalcogenides possess a high piezoelectric coefficient, and additional out of plane piezoelectric coefficients were found in Janus group III monochalcogenides due to induces out of plane dipolar polarization caused by breaking mirror symmetry.[20] In this work, we systematically investigate the effect of spin–orbit coupling (SOC) on the electronic, optical, and thermoelectric properties of Janus Ga_2SSe monolayer by mean of DFT calculations. We focus on the influence of SOC on the band structure and band gap of Ga_2SSe. Optical characteristics and electronic transport coefficients are calculated and discussed in detail when the SOC was included.

2 Computational details

The projector augmented wave method is used within the DFT calculations as implemented in the Quantum ESPRESSO code.[21] The Perdew–Burke–Ernzerhof (PBE) functional[22] with the spin–orbit coupling (SOC)[23] of the generalized gradient approximation (GGA) is used to consider the interaction of the exchange-correlation. A $15 \times 15 \times 1$ k-point mesh in the Brillouin zone is used for optimization. A vacuum space in the c direction was set to be 20 Å to avoid any artificial interactions between neighbor plates. All self-consistent calculations and geometric optimization are completed until the difference in energy between the forces on each atom and the electron steps converge to be 10^{-3} eV Å^{-1} and 10^{-6} eV, respectively.

A large supercell of $4 \times 4 \times 1$ is used for the calculations of the phonon spectrum to obtain more accurate results. The thermal stability is tested by the *ab initio* molecular dynamics (AIMD) simulations[24] performing through the Nose-thermostat algorithm. Both PBE and PBE + SOC methods are used to study the thermoelectric properties. A $90 \times 90 \times 1$ k-point mesh is used for calculations of the electronic transport properties. The canonical ensemble (NVT) with constant temperature is used for the calculations of the thermoelectric properties. The electronic transport coefficients are estimated by using the semi-classical Boltzmann transport theory within the constant scattering time and rigid band approximations as performed in the BoltzTrap.[25] The Phono3py package[26] has been used to calculate the lattice thermal conductivity.

3 Results and discussion

By replacing one chalcogen atom by another, we can build the Janus Ga_2SSe monolayer from either GaS or GaSe. While both GaS and GaSe belong to the $P\bar{6}m2$ (D_{3h}) space group with mirror symmetry, the lattice of Ga_2SSe has the $P3m1$ (C_{3v}) crystal symmetry. The absence of mirror symmetry in the geometrical structure of Ga_2SSe is expected to give it many novel properties that do not exist in pure monochalcogenides GaSe or GaS. In Fig. 1(a), we show the geometrical structure of Ga_2SSe monolayer at equilibrium. Our calculations revealed that the lattice constant of Ga_2SSe after full relaxation is $a = 3.728$ Å, which is larger/smaller than that of GaS/GaSe. The lacking of out-plane mirror symmetry in Janus Ga_2SSe is due to the difference between Ga–S and Ga–Se bond lengths. Ga–S and Ga–Se bond lengths are respectively 2.387 Å and 2.472 Å. Structural parameters, such as the lattice constant or the bond length, of a material depend on the size of the elements in the material. The difference in the lattice constants between Janus structure Ga_2SSe and pure monochalcogenides GaS and GaSe is due to the difference in the size of the chalcogen atom in these compounds. The structural parameters of Ga_2SSe are listed in Table 1.

Table 1 The calculated lattice constant a, thickness h, bond lengths d, and the S–Ga–Ga and Ga–Ga–Se bond angles ϕ of Ga_2SSe monolayer

	a (Å)	d_{Ga-S} (Å)	d_{Ga-Se} (Å)	d_{Ga-Ga} (Å)	h (Å)	$\phi_{\angle SGaGa}$ (deg.)	$\phi_{\angle GaGaSe}$ (deg.)
GaS	3.585	2.471	—	2.457	4.651	117.375	—
GaSe	3.818	—	2.497	2.468	4.814	—	117.965
Ga_2SSe	3.728	2.387	2.472	2.465	4.725	115.762	119.637

This journal is © The Royal Society of Chemistry 2020

Open Access Article. Published on 17 December 2020. Downloaded on 7/16/2025 6:28:26 AM.
This article is licensed under a Creative Commons Attribution-NonCommercial 3.0 Unported Licence.

The structural stability of material can be attested through an analysis of its phonon dispersion relations. The structure is dynamically stable when its phonon modes throughout the Brillouin zone have a positive frequency. The restoring force, which counteracts the displacement of atoms, is lost if there are negative frequencies in the phonon spectrum. The phonon dispersion relations of Ga_2SSe monolayer is shown in Fig. 1(b). We can see that there are 12 vibrational branches in the phonon spectrum of Ga_2SSe. Three optical branches are the longitudinal, transverse, and flexural branches. There is an intersection between the optical branches and the acoustic branches. There are nine optical modes, including three nondegenerate modes and three doubly degenerate at the Γ-point. Most importantly, no soft modes are found in the phonon dispersion curves of Ga_2SSe. This confirms that Ga_2SSe is dynamically stable and we can synthesize Ga_2SSe as a free-standing monolayer.

While dynamical stability is a guarantee for a material to be physically viable, thermal stability is a necessary condition for that material to be applied in real equipment. To test the thermal stability, the time-dependence of the temperature fluctuation of Ga_2SSe is calculated by AIMD simulations and the obtained result is presented in Fig. 1(c). Our calculated results demonstrated that there is no significant distortion in the atomic structure of Ga_2SSe after 5 ps (with 5000 time-steps) of heat-treatment at room temperature. There is no bond-breaking as well as no structural reconstruction in Ga_2SSe after heating, warranting its thermal stability.

In Fig. 2, we show our calculated results for band structure, which is plotted along the Γ–M–K–Γ direction, and partial density of states (PDOS) of Ga_2SSe at equilibrium using both PBE and PBE-SOC methods. From Fig. 2(a), we can see that the Janus Ga_2SSe is an indirect semiconductor with the conduction band minimum (CBM) and valence band maximum (VBM) locating respectively at M-point and on MK-path. At the PBE level, the indirect band gap of Ga_2SSe is $E_g^{K\rightarrow MK} = 2.070$ eV. However, the direct band gap by PBE functional is very close to the indirect one, $E_g^{K\rightarrow MK} = 2.183$ eV, as depicted in Fig. 2(a). This implies that the change of position of the VBM can take place when the Janus monolayer is influenced by external factors such as strain engineering or external electric field.

It is well-known that the SOC effect plays a key role in determining the electronic properties of materials, especially in the case of compounds containing heavy elements. The heavier the element-containing material, the greater the influence of the SOC on the electronic properties of that material. When the SOC effect was included, the band structure was significantly altered as shown in Fig. 2(b). By comparing Fig. 2(a) and (b), we can see that there are splitting bands in the band structure of Ga_2SSe due to the spin–orbit coupling. Our calculations revealed that the SOC effect slightly reduced the band gap of Ga_2SSe, from 2.070 eV (without SOC) to 2.050 eV (with SOC). Also, small spin–orbit splitting energy of $\Delta = 90$ meV is found in the valence band at the M-point in the Brillouin zone. Due to the size of elements, the spin–orbit splitting energy Δ in Ga_2SSe is smaller than that in other compounds in the same group III such as Ga_2SeTe (416 meV).[9] This difference in spin–orbit splitting energy is due to the difference in size between the S and Te elements. In Fig. 2(c), we show our calculations for the partial density of states (DOS) of Ga_2SSe by PBE + SOC method. Based on the analysis of the PDOS, we can estimate the contribution of the atom orbital to the electronic bands of Ga_2SSe. We can see that the S-p and Se-p orbitals have a great contribution to the valence band. For the atom orbitals of Ga, the Ga-s orbital has a dominant contribution to the conduction band while the valence band receives significant contributions from the Ga-p orbital. In Fig. 3, we plot the weighted band structure of Ga_2SSe, which can help to estimate the contribution of atomic orbital to the CBM and VBM. We show only the s- and p-orbitals of the atoms because the d-orbital contributes to the higher energy region. From Fig. 3, we can see that the VBM is largely contributed from the S-d and Se-d orbitals while the Ga-s and S-s orbitals significantly contribute to the CBM.

Electronic bands of 2D materials are sensitive to the change in geometrical structure. Therefore, strain engineering is one of the best ways to drive the electronic properties of 2D materials.

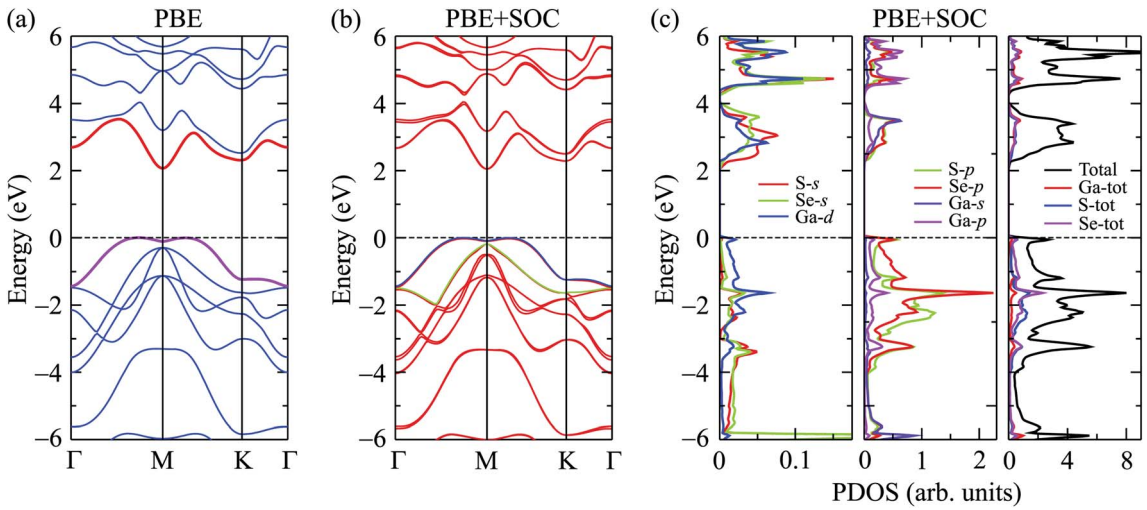

Fig. 2 Calculated band structures of Ga_2SSe by PBE (a) and PBE + SOC (b) methods. (c) PDOS of Ga_2SSe by PBE + SOC method.

Open Access Article. Published on 17 December 2020. Downloaded on 7/16/2025 6:28:26 AM.
This article is licensed under a Creative Commons Attribution-NonCommercial 3.0 Unported Licence.

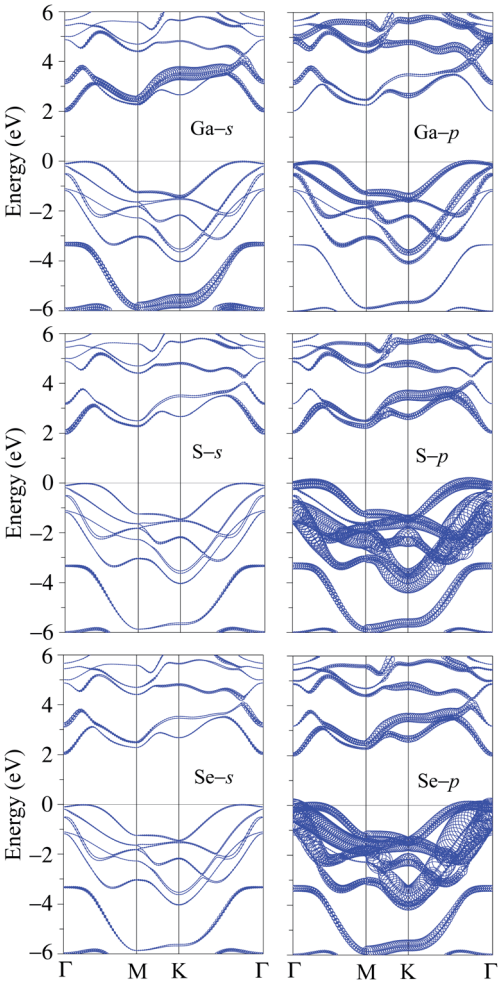

Fig. 3 Weighted band structures of Ga_2SSe monolayer.

The band structure of Ga_2SSe under different values of biaxial strain ε_b is shown in Fig. 4. The band structure of Ga_2SSe changes interestingly in the presence of strain. When compressive strain is applied, the band structure of Ga_2SSe changes perfectly as shown in Fig. 4(a). The VBM tends to shift to the *M*-point of the Brillouin zone. At the same time, the CBM tends to shift away from the *M*-point and towards the *K*-point. The consequence of this is that Ga_2SSe remains an indirect semiconductor under the compressive strain even though the VBM moves to the *M*-point when $\varepsilon_b = -3\%$. The influence of the tensile strain $\varepsilon_b > 0$) on the band structure of Ga_2SSe is depicted in Fig. 4(b). From Fig. 4(b), we can see that Ga_2SSe is still the indirect semiconductor in the whole tensile strain range with the CBM and VBM located at *M*-point and *MK*-path, respectively. However, the band gap of Ga_2SSe decreases significantly with increasing tensile strain. The band gap of Ga_2SSe decreases almost linearly with increasing tensile strain as shown in Fig. 5(a). Meanwhile, the compressive strain not only significantly changed the band structure of Ga_2SSe as above-mentioned, but also changed its band gap irregularly. In the presence of the compressive strain, the band gap increases to the maximum value at $\varepsilon_b = 3\%$ and then decreases again with

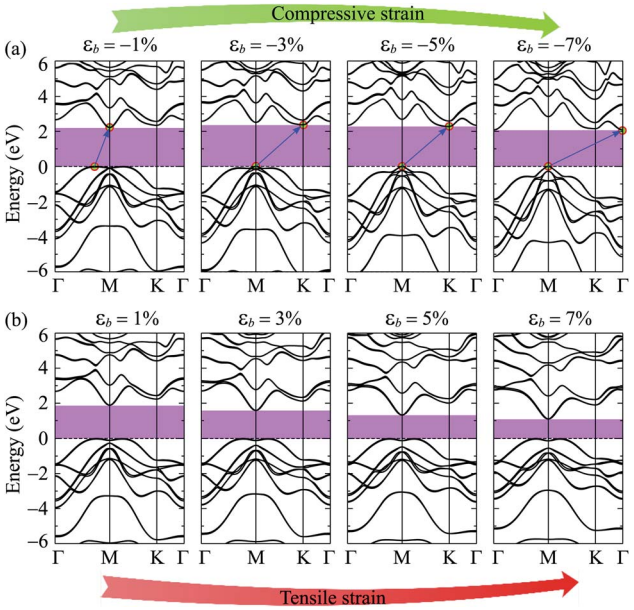

Fig. 4 Band structure of Ga_2SSe under the compressive (a) and tensile (b) strains.

a continued increase in compressive strain. More interestingly, while the difference in band gap calculated by PBE and PBE + SOC methods is quite small in the case of tensile strain, there is a clear difference between them in the case of compressive strain, especially in large compressive strain. The maximum value of the calculated band gap by PBE and PBE + SOC methods is 2.488 eV and 2.376 eV, respectively. In Fig. 5(b), we depict the biaxial strain dependence of spin–orbit splitting

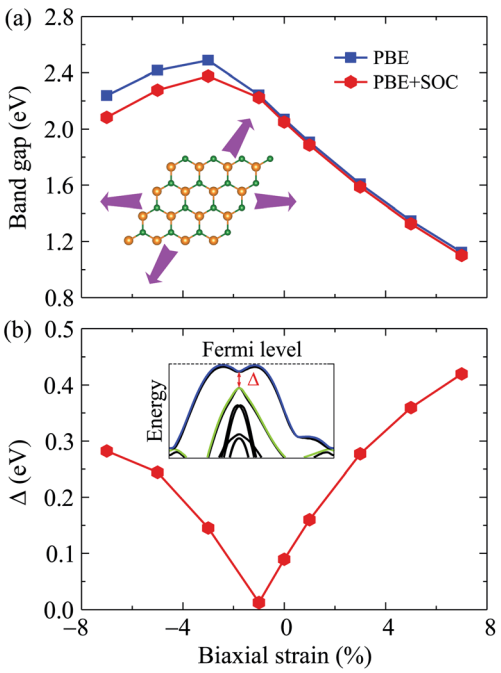

Fig. 5 Band gap (a) and spin–orbit splitting energy Δ (b) of Ga_2SSe as a function of biaxial strain.

This journal is © The Royal Society of Chemistry 2020

Open Access Article. Published on 17 December 2020. Downloaded on 7/16/2025 6:28:26 AM.
This article is licensed under a Creative Commons Attribution-NonCommercial 3.0 Unported Licence.

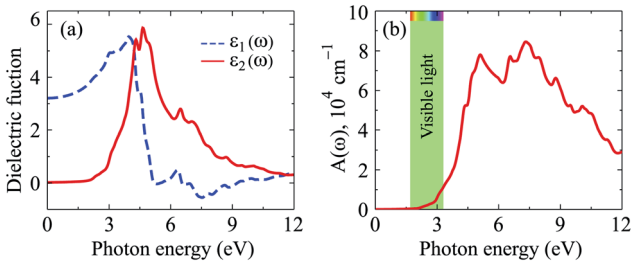

Fig. 6 (a) Calculated the dielectric function and (b) optical absorption coefficient of Ga_2SSe monolayer by PBE + SOC method.

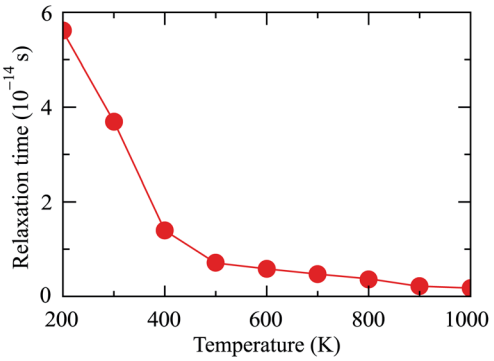

Fig. 7 Calculated temperature-dependent relaxation time of Ga_2SSe monolayer by PBE + SOC method.

energy Δ. As above-mentioned, the spin–orbit splitting energy Δ in Ga_2SSe is quite small at equilibrium (only 90 meV), however, Δ decreases rapidly with the increasing of the tensile strain. The spin–orbit splitting energy is up to 419 meV at $\varepsilon_b = 7\%$. On the other hand, the spin–orbit splitting energy depends dramatically on the compressive strain. When the compressive strain strength increases, the splitting energy Δ decreases to 12 meV at $\varepsilon_b = -1\%$ and then increases again. It is clear that the structural strain has drastically changed the electronic structure of the Janus Ga_2SSe, not only the band gap but also the spin–orbit splitting energy.

We next study the optical properties of the Janus Ga_2SSe. The incoming photon is parallel polarized and a large range of photon energy $\hbar\omega$ from 0 eV to 12 eV is investigated in this work. The fundamental optical characteristics can be studied through the dielectric function as $\varepsilon(\omega) = \varepsilon_1(\omega) + i\varepsilon_2(\omega)$. The imaginary part $\varepsilon_2(\omega)$ is usually calculated first by summing of the filled–unfilled state transitions:[27,28]

$$\varepsilon_2{}^{ij}(\omega) = \frac{4\pi^2 e^2}{Vm^2\omega^2}\sum_{mm'\sigma}\langle kn\sigma|p_i|kn'\sigma\rangle \times f_{kn}(1-f_{kn'})$$

$$\delta(E_{kn'} - E_{kn} - \hbar\omega), \quad (1)$$

where m and e are the mass and charge of an electron, respectively, ω is the incoming light angular frequency, V is the unit cell volume, $|knp\rangle$ is the wavefunction of the crystal with momentum p, and f_{kn} is the Fermi distribution function. The real part $\varepsilon_1(\omega)$ can then derive *via* the Kramer–Kronig relation[27,28]

$$\varepsilon_1(\omega) = 1 + \frac{2}{\pi}P\int_0^\infty \frac{\omega'\varepsilon_2(\omega')}{\omega'^2 - \omega^2}d\omega'. \quad (2)$$

The optical absorption coefficient $A(\omega)$ can be derived from the parts of $\varepsilon(\omega)$ as the follows:[29]

$$A(\omega) = \frac{\sqrt{2}\omega}{c}\left[\sqrt{\varepsilon_1{}^{ij}(\omega)^2 + \varepsilon_2{}^{ij}(\omega)^2} - \varepsilon_1{}^{ij}(\omega)\right]^{1/2}. \quad (3)$$

The calculated dielectric function by the PBE + SOC method is presented in Fig. 6(a). We can see that Ga_2SSe exhibits low static dielectric constant $\varepsilon_1(0)$. At equilibrium, Ga_2SSe has $\varepsilon_1(0) = 3.209$, which is lower than that of Ga_2STe[30] or Ga_2SeTe.[9] This is consistent with Penn model,[31] which claims that static dielectric constant is inversely proportional to direct bandgap of materials. The optical characteristics is strongly connected to the $\varepsilon_2(\omega)$, which is also presented in Fig. 6(a). As shown in Fig. 6(a), it is found that the first peak in $\varepsilon_2(\omega)$ spectrum is located at the incoming light energy $\hbar\omega = 4.313$ eV. The main peak in $\varepsilon_2(\omega)$ is also located in the near-ultraviolet region, at $\hbar\omega = 4.640$ eV. These optical peaks are related to the optical absorbance peaks, which are shown in Fig. 6(b). Optical absorption in Ga_2SSe is activated in the visible light region (at $\hbar\omega \approx 2$ eV) then absorption intensity rapidly increases. The maximum intensity in the visible region is up to 1.2×10^4 cm^{-1}. The first absorption peak is at $\hbar\omega = 5.102$ eV in the near-ultraviolet region. Ga_2SSe exhibits great absorption intensity in the near-ultraviolet region. The maximum absorption intensity is up to $A(\omega) = 8.444 \times 10^4$ cm^{-1} at $\hbar\omega = 7.334$ eV.

In the last part of this work, we consider the electronic transport coefficients of Ga_2SSe monolayer. Previously, Hicks and Dresselhaus have indicated that low-dimensional nanostructures can be thermoelectric materials.[32] We focus on the basic electronic transport coefficients, including the Seebeck coefficient S, electrical conductivity σ, power factor $S^2\sigma$, and figure of merit ZT, which are all calculated by PBE + SOC method.

The relaxation time τ is a key parameter of the electronic transport features. The τ depends highly on the scattering processes in the materials. Hence, we assume that τ does not dependent on the doping level N. In the present work, the EPW package[33] interfaced with Quantum ESPRESSO[21] is used to estimate the relaxation time. Obtained results demonstrate that the relaxation time of Ga_2SSe at room temperature ($T = 300$ K) is 3.63×10^{-14} s. This value is close to the previous report for MoS_2 being 5.17×10^{-14} s.[34] The dependence of the relaxation time on temperature T is shown in Fig. 7. From Fig. 7, it is revealed that the smaller the relaxation time in the higher the temperature region.

Based on the electronic band structures, the electronic transport coefficients have been calculated by using the Boltzmann transport equation within the constant scattering time approximation *via* the BoltzTraP package.[25] The electronic transport properties can be built from the transport distribution Ξ, which can be obtained from the band structure of material[35]

Open Access Article. Published on 17 December 2020. Downloaded on 7/16/2025 6:28:26 AM.
This article is licensed under a Creative Commons Attribution-NonCommercial 3.0 Unported Licence.

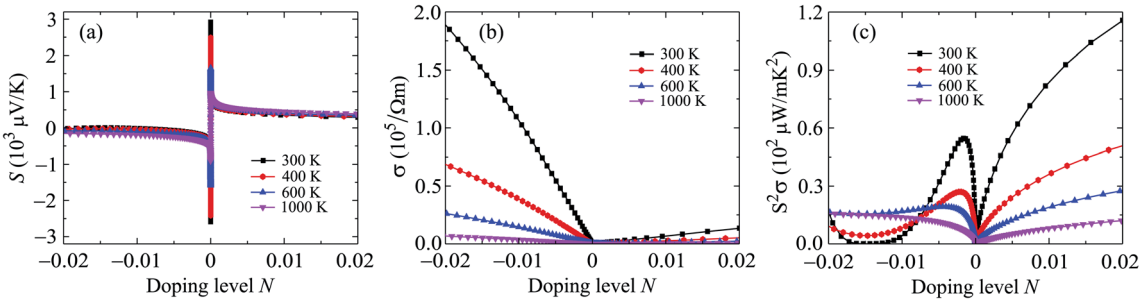

Fig. 8 Seebeck coefficient S (a) electrical conductivity σ (b), and power factor $S^2\sigma$ (c) of Ga_2SSe at different values of temperature.

$$\Xi = \sum_{\vec{k}} \vec{v}_{\vec{k}}^{\alpha} \vec{v}_{\vec{k}}^{\beta} \tau_{\vec{k}}, \tag{4}$$

where $\vec{v}^{\alpha/\beta}$ stands for the group velocity of the carrier with the wavevector $\vec{k}$ and τ is the carrier relaxation time. The electrical conductivity σ, electronic thermal conductivity κ_e, and the Seebeck coefficient S are given by[35]

$$\sigma = e^2 \int \left(-\frac{\partial f_0}{\partial \varepsilon} \right) \Xi(\varepsilon) \mathrm{d}\varepsilon, \tag{5}$$

$$\kappa_e = \frac{1}{T} \int \left(-\frac{\partial f_0}{\partial \varepsilon} \right) (\varepsilon - \mu)^2 \Xi(\varepsilon) \mathrm{d}\varepsilon, \tag{6}$$

$$S = \frac{e k_B}{\sigma} \int \left(-\frac{\partial f_0}{\partial \varepsilon} \right) \frac{\varepsilon - \mu}{k_B T} \Xi(\varepsilon) \mathrm{d}\varepsilon, \tag{7}$$

where e is the electron charge, μ is the chemical potential, k_B is the Boltzmann constant, and f_0 is the Bose–Einstein distribution function.

In the nanostructures, the number of holes/electrons per unit cell or the doping level N has been used instead of doping concentration. The positive/negative value of N refers to the p/n-type doping. In Fig. 8, we show the calculated results for the Seebeck coefficient, electrical conductivity, power factor, and electronic thermal conductivity of Ga_2SSe monolayer at different values of temperature by using the PBE + SOC method. As shown in Fig. 8, we can see that the Seebeck coefficient and electrical conductivity σ of Ga_2SSe for the p-type doping depend weakly on temperature while the power factor of Ga_2SSe monolayer depends strongly on temperature, especially in the p-doping case. The electrical conductivity decreases markedly with increasing temperature in the case of n-type doping.

The key factor of thermal nanomaterials is the figure of merit ZT, which is evaluated by the expression[36]

$$ZT = S^2 \sigma T \frac{1}{\kappa_e + \kappa_l}, \tag{8}$$

where κ_e and κ_l are the electronic and lattice thermal conductivity, respectively.

From eqn (8), we reveal that the magnitude of the total thermal conductivity κ_{tot} ($\kappa_{tot} = \kappa_e + \kappa_l$), especially the lattice part κ_l, is considered as a key factor in determining the value of the figure of merit ZT. In our calculations, the assumption of κ_l independent of the doping level N has been used, which has been properly proven in previous works.[34,37] The thermal conductivity of Ga_2SSe is depicted in Fig. 9. Our obtained results demonstrate that both κ_e and κ_l depend highly on temperature. As shown in Fig. 9(b), the Janus Ga_2SSe exhibits a very low κ_l. The κ_l of Ga_2SSe is only 0.028 W mK^{-1} at room temperature and it decreases with the increasing temperature. The N-dependent total thermal conductivity κ_{tot} at different values of temperature is shown in Fig. 9(b). We can see that the κ_{tot} decreases with the increasing temperature for both cases of doping type.

Possessing very low κ_l, Ga_2SSe is expected to have a high ZT, particularly in the high-temperature region. The calculated results for the dependence of ZT on the doping level N by the PBE + SOC method are presented in Fig. 10. At room temperature, the maximum ZT is up to 0.725 for the p-type doping. The value of ZT for the p-type doping is higher than that for the case

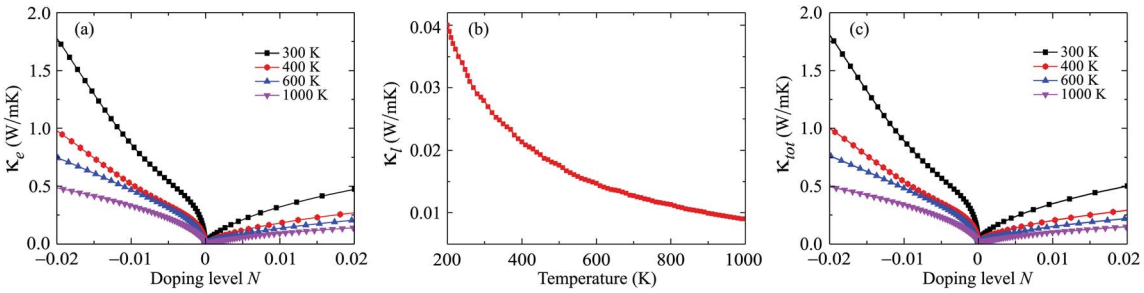

Fig. 9 (a) Doping level dependence of electronic conductivity κ_e, (b) temperature dependent lattice thermal conductivity κ_l, and (c) doping level dependence of total thermal conductivity κ_{tot} of Ga_2SSe monolayer.

 This journal is © The Royal Society of Chemistry 2020

Open Access Article. Published on 17 December 2020. Downloaded on 7/16/2025 6:28:26 AM.
This article is licensed under a Creative Commons Attribution-NonCommercial 3.0 Unported Licence.

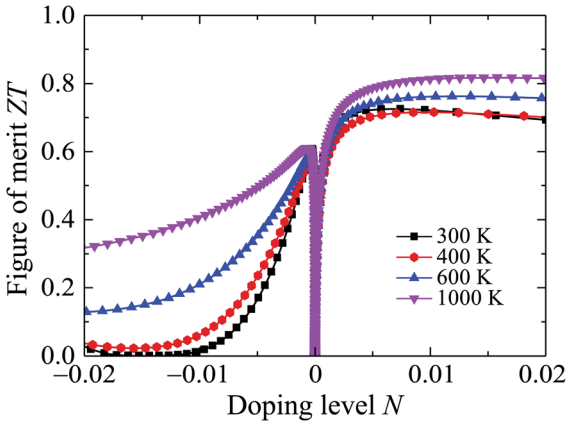

Fig. 10 Doping level dependent figure of merit *ZT* of Ga_2SSe at different values of temperature.

of the p-type doping and we can increase *ZT* by temperature. In the doping level ranging from 0 to 0.02, the *ZT* of Ga_2SSe can be increased to 0.817 at 1000 K. With very low thermal conductivity and high *ZT*, Ga_2SSe has great potential for applications as thermoelectric materials.

4 Conclusion

In conclusion, we present a systematic investigation of the electronic, optical, and thermoelectric properties of Ga_2SSe by using DFT calculations. The Janus Ga_2SSe was confirmed to be dynamical and thermal stabilities *via* the phonon analysis and AIMD simulations. It is found that Ga_2SSe exhibits an indirect characteristic semiconductor and its band gap can be driven by biaxial strain. The SOC not only reduces the band gap but also causes a small spin–orbit splitting of 90 meV in the valence band. The optical absorption spectrum of Ga_2SSe is activated in the visible light and the first peak of the absorption spectrum locates in the near-ultraviolet region. With high absorption intensity, Ga_2SSe is expected to have great potential for applications in optoelectronics. By solving the Boltzmann transport equations, the electronic transport coefficients have been investigated. Both PBE and PBE + SOC methods are used to calculate the electronic transport coefficients. Monolayer Ga_2SSe exhibits a high *ZT* at room temperature and its *ZT* can be enhanced by temperature.

Conflicts of interest

There are no conflicts to declare.

Acknowledgements

This research is funded by Funds for Science and Technology Development of the University of Danang under project number B2019-DN03-43.

References

1 N. A. Poklonski, S. A. Vyrko, A. I. Siahlo, O. N. Poklonskaya, S. V. Ratkevich, N. N. Hieu and A. A. Kocherzhenko, *Mater. Res. Express*, 2019, **6**, 042002.
2 A. I. Siahlo, N. A. Poklonski, A. V. Lebedev, I. V. Lebedeva, A. M. Popov, S. A. Vyrko, A. A. Knizhnik and Y. E. Lozovik, *Phys. Rev. Mater.*, 2018, **2**, 036001.
3 N. Poklonski, E. Kislyakov, N. N. Hieu, O. Bubel', S. Vyrko, A. Popov and Y. Lozovik, *Chem. Phys. Lett.*, 2008, **464**, 187.
4 A.-Y. Lu, H. Zhu, J. Xiao, C.-P. Chuu, Y. Han, M.-H. Chiu, C.-C. Cheng, C.-W. Yang, K.-H. Wei, Y. Yang, Y. Wang, D. Sokaras, D. Nordlund, P. Yang, D. A. Muller, M.-Y. Chou, X. Zhang and L.-J. Li, *Nat. Nanotechnol.*, 2017, **12**, 744.
5 J. Zhang, S. Jia, I. Kholmanov, L. Dong, D. Er, W. Chen, H. Guo, Z. Jin, V. B. Shenoy, L. Shi and J. Lou, *ACS Nano*, 2017, **11**, 8192–8198.
6 Y. Sun, Z. Shuai and D. Wang, *Nanoscale*, 2018, **10**, 21629.
7 D. D. Vo, T. V. Vu, N. V. Hieu, N. N. Hieu, H. V. Phuc, N. T. T. Binh, L. T. T. Phuong, M. Idrees, B. Amin and C. V. Nguyen, *Phys. Chem. Chem. Phys.*, 2019, **21**, 25849.
8 S.-D. Guo, X.-S. Guo, R.-Y. Han and Y. Deng, *Phys. Chem. Chem. Phys.*, 2019, **21**, 24620.
9 T. V. Vu, V. T. T. Vi, C. V. Nguyen, H. V. Phuc and N. N. Hieu, *J. Phys. D: Appl. Phys.*, 2020, **53**, 455302.
10 S.-D. Guo, X.-S. Guo and Y. Deng, *J. Appl. Phys.*, 2019, **126**, 154301.
11 A. Huang, W. Shi and Z. Wang, *J. Phys. Chem. C*, 2019, **123**, 11388.
12 Q.-F. Yao, J. Cai, W.-Y. Tong, S.-J. Gong, J.-Q. Wang, X. Wan, C.-G. Duan and J. H. Chu, *Phys. Rev. B*, 2017, **95**, 165401.
13 J. Yuan, Y. Shan and T. Li, *J. Phys. D: Appl. Phys.*, 2020, **53**, 125502.
14 T. V. Vu, H. D. Tong, D. P. Tran, N. T. T. Binh, C. V. Nguyen, H. V. Phuc, H. M. Do and N. N. Hieu, *RSC Adv.*, 2019, **9**, 41058.
15 X. Yang, D. Singh, Z. Xu, Z. Wang and R. Ahuja, *J. Mater. Chem. C*, 2019, **7**, 12312–12320.
16 T. V. Vu, N. V. Hieu, H. V. Phuc, N. N. Hieu, H. Bui, M. Idrees, B. Amin and C. V. Nguyen, *Appl. Surf. Sci.*, 2020, **507**, 145036.
17 H. T. T. Nguyen, M. M. Obeid, A. Bafekry, M. Idrees, T. V. Vu, H. V. Phuc, N. N. Hieu, L. T. Hoa, B. Amin and C. V. Nguyen, *Phys. Rev. B*, 2020, **102**, 075414.
18 X. Cheng, C. Zhang, L. Guan and J. Tao, *Phys. Status Solidi B*, 2019, **256**, 1900070.
19 W. Wan, S. Zhao, Y. Ge and Y. Liu, *J. Phys.: Condens. Matter*, 2019, **31**, 435501.
20 Y. Guo, S. Zhou, Y. Bai and J. Zhao, *Appl. Phys. Lett.*, 2017, **110**, 163102.
21 P. Giannozzi, S. Baroni, N. Bonini, M. Calandra, R. Car, C. Cavazzoni, D. Ceresoli, G. L. Chiarotti, M. Cococcioni, I. Dabo, A. D. Corso, S. de Gironcoli, S. Fabris, G. Fratesi, R. Gebauer, U. Gerstmann, C. Gougoussis, A. Kokalj, M. Lazzeri, L. Martin-Samos, N. Marzari, F. Mauri, R. Mazzarello, S. Paolini, A. Pasquarello, L. Paulatto,

Open Access Article. Published on 17 December 2020. Downloaded on 7/16/2025 6:28:26 AM.
This article is licensed under a Creative Commons Attribution-NonCommercial 3.0 Unported Licence.

C. Sbraccia, S. Scandolo, G. Sclauzero, A. P. Seitsonen, A. Smogunov, P. Umari and R. M. Wentzcovitch, *J. Phys.: Condens. Matter*, 2009, **21**, 395502.

22 J. P. Perdew, K. Burke and M. Ernzerhof, *Phys. Rev. Lett.*, 1996, **77**, 3865.

23 A. H. MacDonald, W. E. Picket and D. D. Koelling, *J. Phys. C: Solid State Phys.*, 1980, **13**, 2675.

24 S. Nosé, *J. Chem. Phys.*, 1984, **81**, 511.

25 G. K. Madsen and D. J. Singh, *Comput. Phys. Commun.*, 2006, **175**, 67.

26 A. Togo, L. Chaput and I. Tanaka, *Phys. Rev. B: Condens. Matter Mater. Phys.*, 2015, **91**, 094306.

27 A. Delin, P. Ravindran, O. Eriksson and J. Wills, *Int. J. Quantum Chem.*, 1998, **69**, 349.

28 S. Z. Karazhanov, P. Ravindran, A. Kjekshus, H. Fjellvag and B. G. Svensson, *Phys. Rev. B: Condens. Matter Mater. Phys.*, 2007, **75**, 155104.

29 P. Ravindran, A. Delin, B. Johansson, O. Eriksson and J. M. Wills, *Phys. Rev. B: Condens. Matter Mater. Phys.*, 1999, **59**, 1776–1785.

30 H. T. T. Nguyen, V. T. Vi, T. V. Vu, H. V. Phuc, C. V. Nguyen, H. D. Tong, L. T. Hoa and N. N. Hieu, *Phys. E*, 2020, **124**, 114358.

31 D. R. Penn, *Phys. Rev.*, 1962, **128**, 2093.

32 L. D. Hicks and M. S. Dresselhaus, *Phys. Rev. B: Condens. Matter Mater. Phys.*, 1993, **47**, 16631(R).

33 S. Poncé, E. Margine, C. Verdi and F. Giustino, *Comput. Phys. Commun.*, 2016, **209**, 116–133.

34 Z. Jin, Q. Liao, H. Fang, Z. Liu, W. Liu, Z. Ding, T. Luo and N. Yang, *Sci. Rep.*, 2015, **5**, 18342.

35 G. Ding, J. He, Z. Cheng, X. Wang and S. Li, *J. Mater. Chem. C*, 2018, **6**, 13269.

36 Y. Pei, X. Shi, A. LaLonde, H. Wang, L. Chen and G. J. Snyder, *Nature*, 2011, **473**, 66.

37 W. Huang, H. Da and G. Liang, *J. Appl. Phys.*, 2013, **113**, 104304.

 This journal is © The Royal Society of Chemistry 2020